Journal of Metals, Materials and Minerals, 36(4), e2632, 2026

Facile stearic acid modifications of alumina nanoparticles for superhydrophobic coating

Noppakhate JIRABORVORNPONGSA[1,2,*], Naris SUPAJANYA[3], and Pornapa SUJARIDWORAKUN[2,4,5]

[1] *Metallurgy and Materials Science Research Institute, Chulalongkorn University, Bangkok 10330, Thailand*
[2] *Center of Excellence on Photocatalysts for Clean Environment and Energy, Faculty of Science, Chulalongkorn University, Bangkok, 10330, Thailand*
[3] *Department of Chemistry, Faculty of Science, Srinakharinwirot University, Bangkok 10110, Thailand*
[4] *Department of Materials Science, Faculty of Science, Chulalongkorn University, Bangkok, 10330, Thailand*
[5] *Center of Excellence on Petrochemical and Materials Technology, Chulalongkorn University, Bangkok 10330, Thailand*

***Corresponding author e-mail**: noppakhate.j@chula.ac.th

Received date:
21 January 2026
Revised date:
26 March 2026
Accepted date:
24 June 2026

Keywords:
Superhydrophobic coating;
Surface modification;
Stearic acid;
Alumina;
Polydimethylsiloxane

Abstract

In this study, alumina nanoparticles were modified with stearic acid (SA) dissolved in ethanol solution via facile techniques, which were soaking and refluxing. The effects of these modification techniques on the thermal behaviors and the functional groups of the SA-modified alumina were investigated. Stearic acid was successfully modified onto alumina nanoparticles using both techniques. In comparison, the refluxing technique yielded a higher degree of SA modification, corresponding to a grafting density of 2.59 molecules·nm^{-2}, which is approximately twice that of the soaking technique. Then, the SA-modified alumina via refluxing technique was mixed with polydimethylsiloxane (PDMS) and spray coated on glass slides. The effects of coating layers and the SA-modified alumina content on the wettability and optical property were studies. The 4-layered coating containing 10 wt% of SA-modified alumina exhibited superhydrophobic property with a water contact angle of 150.0° and the contact angle hysteresis of 6.2°. It also showed excellent self-cleaning performance. However, transmittance of 4-layered coating reduced dramatically. The results showed that increasing the number of coating layers enhanced surface wettability but adversely affected optical transmittance due to increased light scattering. Therefore, a balance between wettability and optical transparency must be considered. These findings indicated that SA-modification effectively enhanced the hydrophobicity of alumina particles, and the incorporation of these SA-modified particles introduced sufficient roughness to further improve hydrophobicity. The progress in the surface modification and the utilization of a spray coating method highlight the potential for scalable and facile fabrication of superhydrophobic coating.

1. Introduction

Superhydrophobic surfaces typically defined as having a water contact angle (WCA) greater than 150° and contact angle hysteresis (CAH) less than 10° have gained significant research interest due to their remarkable functionalities, including self-cleaning, antifouling, anti-icing, and reduced fluid drag [1,2]. These characteristics make superhydrophobic coatings highly desirable for applications in optical devices, self-cleaning windows, traffic indicators, solar panels, and protective coatings [3–6]. However, practical implementation is often hindered by challenges associated with achieving high optical transparency, durability under mechanical wear, environmental sustainability, and cost efficiency [7–9].

The fabrication of superhydrophobic surfaces generally requires two key components: surface roughness and low surface energy [1,10]. In general, a perfectly flat surface coated solely with a low-surface-energy material can only achieve a maximum WCA of approximately 120°, which is insufficient to achieve superhydrophobicity. Therefore, hierarchical micro/nano surface structures must be introduced to transition the surface wettability into the Cassie–Baxter wetting regime, where trapped air pockets reduce the solid-liquid interface and dramatically increase hydrophobicity [11,12].

A widely employed strategy to create such roughness involves incorporating metal oxide nanoparticles such as silica (SiO_2), titanium dioxide (TiO_2), alumina (Al_2O_3), and zinc oxide (ZnO) into polymer matrices [13–16]. These nanoparticles, when deposited onto a substrate, generate micro/nano-scale asperities essential for enhance surface roughness. However, achieving effective roughness is not solely dependent on nanoparticle morphology; rather, surface modification of nanoparticles is often required to improve both hydrophobicity and compatibility with polymer binder. Many inorganic nanoparticles inherently possess hydrophilic surface due to hydroxyl (–OH) groups, which limit their dispersion in hydrophobic resin systems [17]. To address this challenge, many studies have employed low surface energy substances such as fluorocarbon compounds to reduce the surface energy of inorganic nanoparticles [18,19]. However, the use of fluorinated materials raised concerns regarding environmental safety and potential toxicity [20]. Therefore, developing effective fluorine-free surface modification strategies remains an important challenge to overcome [21,22].

Among fluorine-free surface modification substances, stearic acid (SA) stands out as a particularly attractive candidate [23–25]. The chemical structure of SA contains a long alkyl chain that exhibits low surface energy. Moreover, SA could be easily modified onto various metal oxide surfaces due to the chemically bond reaction through interaction between its carboxyl (–COOH) group and surface hydroxyl groups of nanoparticles. Previous studies have demonstrated that SA can effectively hydrophobize inorganic materials, including metal oxide nanoparticles, making it a promising candidate for sustainable coating system. Feng *et al.* modified zinc nano-coating with stearic acid via a soaking method [26]. The Zn-coated samples were soaked into stearic acid ethanol solution at room temperature. The prepared samples showed higher water contact angle due to the lower surface energy from stearic acid modification. Li and Weng modified hydroxyapatite powder with stearic acid in organic mediated solution using a refluxing method [27]. The SA-modified hydroxyapatite was successfully prepared. It has good bioactivity and great properties of inorganic fillers in the organic matrix. Both techniques are simple and effective for modified surface with SA. However, the comparative study of these two different methods on the SA modification performance has not been reported to date.

To apply on substrates, these hydrophobic nanoparticles are commonly incorporated into organic adhesive such as polydimethylsiloxane (PDMS), polyurethane, or epoxy resins [28–32]. The polymer binder serves several functions such as anchors the modified nanoparticles to the substrate, provide mechanical flexibility, enhance durability, and contributes to overall hydrophobicity when combined with low surface energy filler. There are various deposition techniques including spin coating [33], dip coating [14,15], and spray coating [13], have been investigated to distribute these hydrophobic nanoparticles across substrate surface. Among them, spray coating has emerged as one of the most practical and scalable approaches due to its simple operation, low equipment cost, tunable film thickness, suitability for large area substrate, and compatibility with industrial fabrication.

In this study, Al_2O_3 nanoparticles, representative of inorganic nanoparticles, were modified with SA using two different techniques, which were soaking and refluxing. The SA-modified Al_2O_3 particles were subsequently incorporated into a PDMS matrix and deposited onto glass slides via spray coating to fabricate fluorine-free superhydrophobic surfaces. The effects of the modification technique on the chemical functionality and thermal behavior of the SA-modified Al_2O_3 particles were investigated. Furthermore, the influence of coating layers and SA-modified Al_2O_3 particles content on wettability and optical transparency was evaluated. Finally, the durability and self-cleaning performance of the optimized coating were assessed to determine its feasibility for practical applications.

2. Experiment

2.1 Materials

Alumina nanoparticle (Al_2O_3, average diameter of 30 nm, Wuxi Admas technology Co.Ltd.), stearic acid (SA, $C_{18}H_{36}O_2$, reagent grade, 95%, Sigma-Aldrich), ethanol, acetone, n-hexane, polydimethylsiloxane elastomer base (PDMS, Sylgard 184A, Dow Corning, Inc.), curing agent (Slygard 184B, Dow Corning, Inc.), and soda lime glass slides were used in the study without any further purification.

2.2 Surface modifications of stearic acid onto alumina nanoparticles

For the soaking technique, stearic acid was first dissolved into ethanol (100 mL) to obtain a 50 mM SA solution. Then, Al_2O_3 powder (10 g) was added, and the suspension was stirred at room temperature for 30 min, followed by static soaking for 24 h. After the reaction, the modified powder was washed repeatedly with ethanol and dried at 70°C for 24 h in an oven. The resulting sample was designated as SA-soak.

For refluxing technique, Al_2O_3 (10 g) was dispersed in 100 mL of 50 mM SA solution (prepared as described above). Then, the suspension was refluxed at 110°C under continuous stirring for 5 h. After the reaction, the modified powder was washed repeatedly with ethanol and dried at 70°C for 24 h. The obtained sample was denoted as SA-reflux.

2.3 Preparation of PDMS and SA-modified Al_2O_3/PDMS coatings

Prior to coating process, glass slides were cleaned sequentially with acetone, ethanol and deionized water using ultrasonication. The coating solution was prepared by dissolving PDMS elastomer base (4.5 g) in n-hexane (45 g) under stirring. Then, SA-reflux powder was added into the solution at 0 wt%, 1 wt%, and 10 wt%. The suspension was stirred for 30 min, followed by adding the curing agent at a weight ratio of 1:10 with respect to the PDMS elastomer base weight. Then, the resulting coating formulation was sprayed on the glass slide using a spray gun (nozzle diameter of 1.0 mm) under a pressure of 0.2 MPa, with a spray duration of 1 s, and a spray distance of 25 cm. After each coating step, the coated glass was allowed to dry at room temperature before proceeding subsequent layers, up to 4 layers to control the coating thickness. Subsequently, the coated glass was cured in an oven at 140°C for 1 h. The coatings prepared without SA-reflux were designated as PDMS-X, whereas those containing SA-reflux were denoted as AY-X, where X represents the number of coating layers (1 layer, 2 layer, 3 layer, or 4 layer) and Y stands for the SA-reflux content (1 wt% or 10 wt%).

2.4 Characterization

Thermalgravimetric behavior of the powders were analyzed using a simultaneous thermal analysis (STA, Netzch STA 2500 Regulus) at heating rate of $10°C \cdot min^{-1}$ under a N_2 atmosphere. Fourier transform infrared (FTIR) spectra of the powders were record using an IR spectrometer (ThermoFisher Scientific iZ10) via a KBr pellet method. The specific surface area was measured via the Brunauer-Emmett-Teller (BET) method with N_2 adsorption-desorption (Micromeritics 3Flex Surface Characterization Analyzer) at 77 K. The surface morphology of the coatings was examined using scanning electron microscope (SEM, Hitachi SU3500). The optical transmittance of the coatings was measured with a UV–vis spectrophotometer (Horiba Duetta). The static, advancing, and receding water contact angles were determined

using a goniometer (Dataphysics OCA25) with a 5 µL water droplet, and each static WCA measurement was repeated at three different positions on the coating to obtain an average value.

3. Results and discussion

The surface of Al_2O_3 was modified in SA solution using either the soaking or refluxing technique. A schematic illustration of the feasible surface modification mechanism is shown in Figure 1. Firstly, SA was dissolved in ethanol solution. Then, SA grafted onto the alumina surface through a chemisorption mechanism involving the reaction between the carboxyl functional groups (–COOH) of SA and the surface hydroxyl groups (–OH) naturally present on alumina. During the reaction, the –COOH groups underwent dehydration with the surface –OH groups, forming ester-like aluminum carboxylate bonds (Al–OOC–R) and releasing water as a byproduct [26,27,34–36]. This reaction results in the SA molecules being chemically bonded to the alumina surface, with their long hydrophobic alkyl chains oriented outward. The outward alignment of these alkyl chains significantly reduces the surface energy of Al_2O_3, thereby enhancing its hydrophobicity.

Figure 2 presents the thermal behaviors of pristine Al_2O_3, SA-soak, and SA-reflux. Pristine Al_2O_3 exhibited a total weight loss of 3.17%, corresponding to the removal of physically adsorbed water below 200°C and the decomposition of surface contaminants up to 250°C [37]. In contrast, both SA-modified samples exhibited additional weight loss in the range of 400°C to 500°C, attributed to the thermal decomposition of chemically bonded SA [35,38]. The total weight loss increased to 5.22% for SA-soak and 7.48% for SA-reflux, indicating that the refluxing technique provided a higher modification density on the Al_2O_3 surface. This result was consistent with the elevated reaction temperature during reflux, which enhanced esterification efficiency and promoted stronger chemical bonding between SA and the Al_2O_3 surface [35,38]. The presence of stable decomposition peaks further confirms the thermally robust nature of the modified stearate layer.

The FTIR spectra of pristine Al_2O_3, SA-soak, and SA-reflux are shown in Figure 3. For all samples, the absorption bands in the range of 1000 cm^{-1} to 500 cm^{-1} correspond to the characteristic Al–O lattice vibration modes of alumina [39]. The broad band centered at approximately 3450 cm^{-1} is attributed to the stretching vibration of surface Al–OH groups associated with adsorbed molecular water [37,39]. In addition, the peak at 1650 cm^{-1} is assigned to the O–H bending mode, further confirming the presence of adsorbed water on the surface [37]. After modification, both SA-modified samples exhibited new absorption peaks at 2920 cm^{-1} and 2851 cm^{-1}, corresponding to the asymmetric and symmetric vibrations of $–CH_2–$ groups from SA, respectively [25,40]. Meanwhile, the asymmetric vibrations of the carboxylate group (–COO-) appeared at 1561 cm^{-1}, along with the C–H bending vibration at 1468 cm^{-1}, indicating the formation of surface bound stearate species [40,41]. These results confirmed that stearic acid was successfully modified onto the Al_2O_3 surface through chemical bonding.

To quantitatively compare the efficiency of SA modification, the grafting densities of SA were determined. The surface grafting density, defined as the number of SA molecules per unit surface area of the particle surface [42]. The grafting density of SA was calculated from the TG-derived organic content and the BET specific surface area of Al_2O_3 particles, according to Equation (1) as follows:

$$n_{SA} = \frac{W_{SA} \times N_A}{MW_{SA} \times S_{BET}} \quad (1)$$

where n_{SA} is the grafting density of SA ($mol \cdot nm^{-2}$), W_{SA} is the mass fraction of grafted SA ($g \cdot g^{-1}$), N_A is Avogadro's constant (mol^{-1}) and MW_{SA} is the molar weight of the grafted SA molecule (267 $g \cdot mol^{-1}$), and S_{BET} is the specific surface area of Al_2O_3 particles ($m^2 \cdot g^{-1}$).

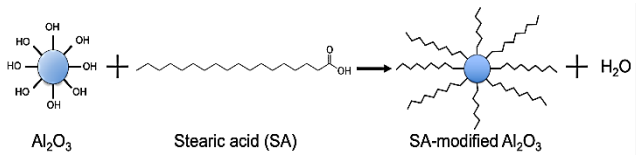

Figure 1. Schematic illustration for the feasible surface modification mechanism.

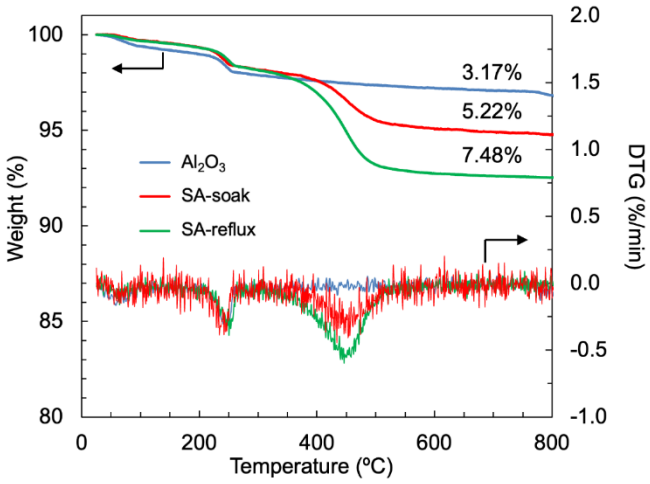

Figure 2. Thermogravimetric (TG) and differential thermogravimetric (DTG) analysis curves of Al_2O_3, SA-soak, and SA-reflux.

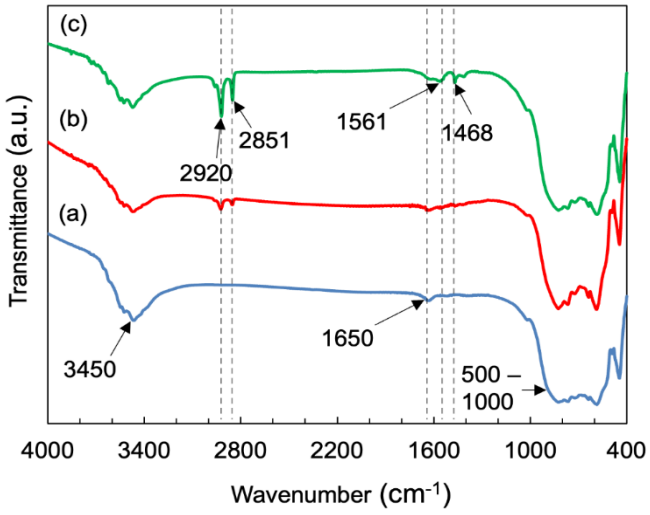

Figure 3. FTIR spectra of sample powders: (a) Al_2O_3, (b) SA-soak, and (c) SA-reflux.

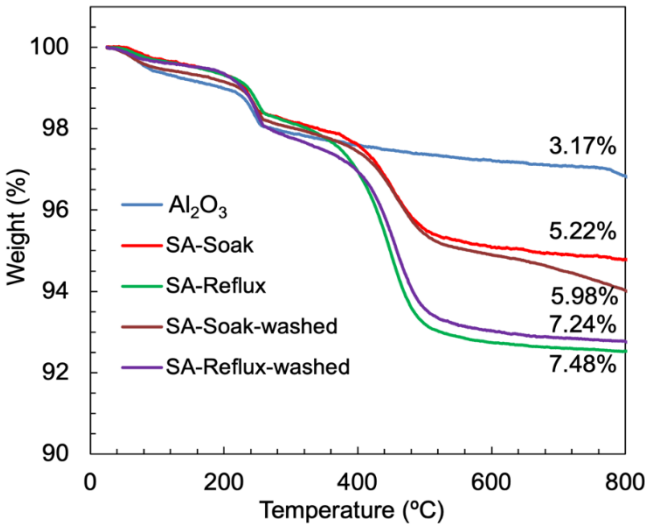

Figure 4. Thermogravimetric (TG) analysis curves of Al_2O_3, SA-soak, SA-reflux, and hexane-washed samples (SA-soak-washed and SA-reflux-washed).

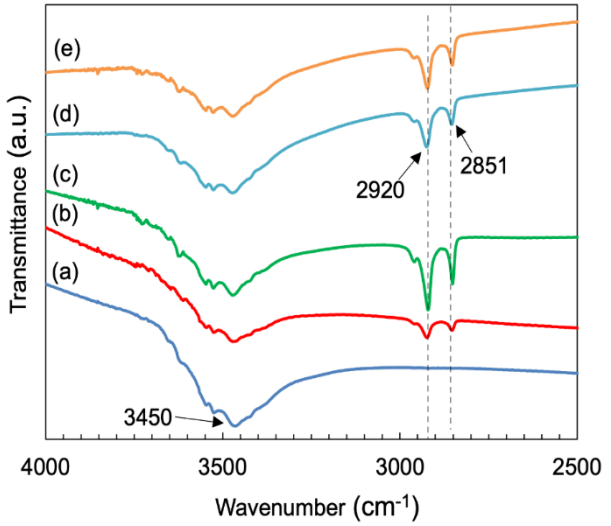

Figure 5. FTIR spectra of sample powders: (a) Al_2O_3, (b) SA-soak, (c) SA-reflux, (d) SA-soak-washed, (e) SA-reflux-washed.

The S_{BET} of Al_2O_3 particle was 37.49 $m^2 \cdot g^{-1}$. The mass fraction of grafted SA was determined from TG results by subtracting the weight loss of pristine Al_2O_3 from that of SA-modified Al_2O_3, to eliminate the contribution from adsorbed water. Based on these values, the grafting densities of SA-soak and SA-reflux were calculated to be approximately 1.23 $mol \cdot nm^{-2}$ and 2.59 $mol \cdot nm^{-2}$, respectively. These results indicated that the refluxing technique yielded approximately twice grafting density compared to the soaking technique.

To further verify the nature of the interaction between SA and the Al_2O_3 surface, an additional washing process was carried out using hexane at 80°C for 5 h to remove any physically adsorbed SA. The TG profiles and the FTIR spectra after washing are presented in Figure 4–5. The total weight loss of the washed SA-modified Al_2O_3 samples did not change significantly compared to that of the unwashed samples. Moreover, the characteristic absorption peaks at 2920 cm^{-1} and 2851 cm^{-1}, corresponding to the asymmetric and symmetric vibrations of $–CH_2–$ groups from SA, remained unchanged. These results suggested that no physically adsorbed SA remained on the SA-modified samples, and that the retained SA was strongly chemically bonded to the Al_2O_3 surface. Moreover, this behavior was observed for both soaking and refluxing techniques. However, the grafting density obtained from the soaking technique was lower than that of the refluxing technique. Consequently, the SA-reflux sample was expected to exhibit enhanced hydrophobicity and was selected as the additive for subsequent coating fabrication.

A mixture of PDMS solution and SA-reflux particles was spray coated on the glass slide. Figure 6 show SEM images of PDMS coating and those containing 10 wt% SA-reflux (A10) with 1 layer and 4 layers. From Figure 6(a–d), the PDMS coatings displayed a smooth and flat morphology without roughness. In contrast, the addition of SA-reflux particles introduced hierarchical micro/nanostructures due to the well-dispersed and partially aggregated particles with an aggregate size of approximately 10 µm. In A10-1, particles coverage on the glass slide was insufficient, leaving an area without particles due to the limited amount of coating solution deposited in a one layer. As the number of coating layers increased to four layers, the particles became more densely packed, forming a continuous hierarchical micro/nano-structure. The SA-reflux particles were bound to the glass surface through the PDMS binder, accumulating layer by layer. During this spray coating process, air pockets could form between successive layers. This hierarchical texture is essential for achieving the Cassie-Baxter wetting state, in which trapped air beneath water droplets enhances water repellency and contributes to the superhydrophobic behavior [12].

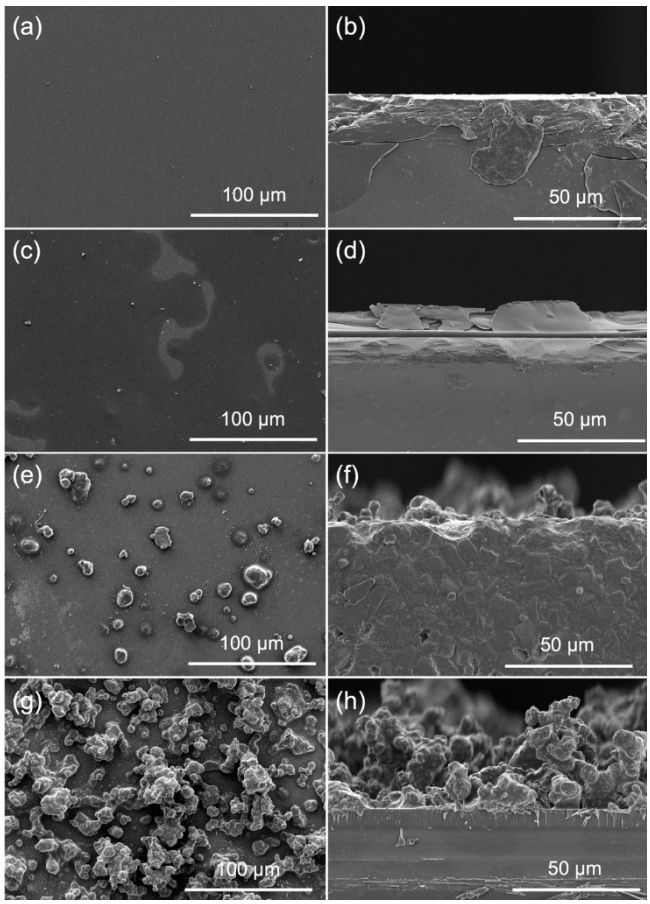

Figure 6. SEM micrographs of the coatings: (a–b) PDMS-1, (c–d) PDMS-4, (e–f) A10-1, and (g–h) A10-4.

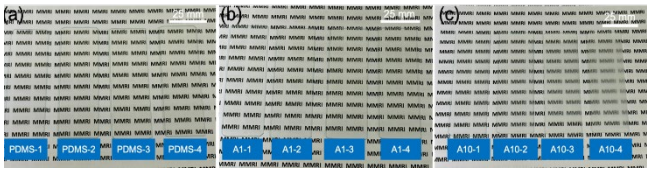

Figure 7. Optical photographs of the coatings: (a) PDMS coatings, (b) A1 coatings, and (c) A10 coatings.

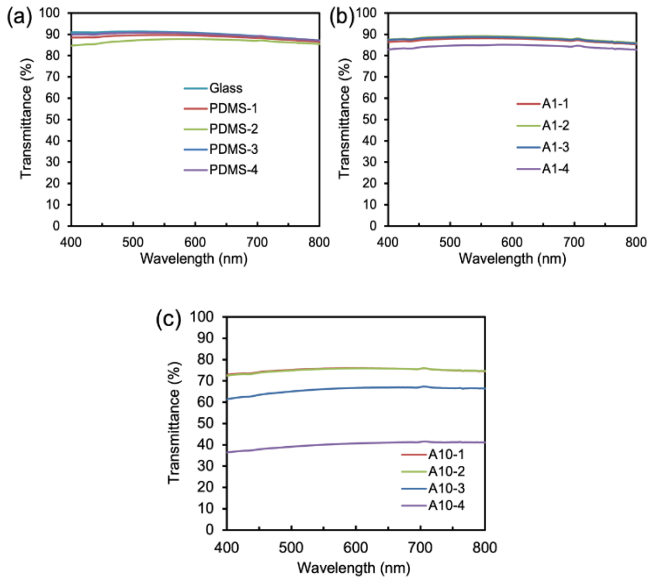

Figure 8. Transmittance spectra of the coatings: (a) PDMS coatings, (b) A1 coatings, and (c) A10 coatings.

Table 1. Average transmittance, water contact angle, and contact angle hysteresis of prepared coating.

Sample name	Average transmittance [%]	Water contact angle [°]	Contact angle hysteresis [°]
Glass	90.2	38.3 ± 3,3	10.8 ± 3.4
PDMS-1	88.8	101.3 ± 1.0	36.8 ± 9.2
PDMS-2	86.8	103.0 ± 0.6	28.1 ± 8.4
PDMS-3	89.9	106.8 ± 1.9	31.8 ± 5.0
PDMS-4	89.7	108.5 ± 0.6	13.0 ± 5.3
A1-1	87.3	102.4 ± 1.9	19.1 ± 6.1
A1-2	88.2	108.7 ± 4.4	15.0 ± 6.0
A1-3	87.8	110.3 ± 2.0	13.6 ± 7.5
A1-4	84.3	112.2 ± 1.6	14.6 ± 6.8
A10-1	75.1	120.2 ± 1.5	27.7 ± 7.1
A10-2	75.1	118.3 ± 1.9	14.1 ± 6.2
A10-3	65.8	146.4 ± 1.2	2.8 ± 2.3
A10-4	40.0	150.0 ± 0.3	6.2 ± 4.2

Figure 7–8 show optical photographs and transmittance spectra of the coatings. From the photographs, PDMS and A1 coatings appeared transparent, allowing the underlying text to be clearly read. In contrast, A10 coatings exhibited noticeable blurriness. The average transmittance (400 nm to 800 nm) of all coatings is listed in Table 1. The average transmittance of the bare glass was 90.2%. Meanwhile, the average transmittance of PDMS and A1 coatings ranged from 86.8% to 89.9%, which is nearly comparable to that of the bare glass. Only the A1-4 coating that showed a slightly lower average transmittance at 84.3%, likely due to its greater coating thickness and higher number of SA-reflux particles. In contrast, A10 coatings exhibited a clear reduction in transmittance, ranging from 40.0% to 75.1%, which became more significant as the number of coating layers increased. This decline in transmittance indicated that greater coating thickness and a higher density of SA-reflux particles enhanced light scattering [43]. The scattering originated from the hierarchical micro/nanostructures, particularly the aggregated particles with sizes approximately of 10 µm. According to the Mie scattering mechanism, particles with sizes comparable to or larger than visible wavelengths induce strong scattering, thereby decreasing transmittance [44,45]. Thus, although increasing the particle content could enhance hydrophobicity by increasing surface roughness, it simultaneously compromises optical transparency. A balance between the particle content and optical properties must therefore be carefully optimized depending on the intended applications.

The water contact angles (WCA) and contact angle hysteresis (CAH) of the coatings are summarized in Table 2. As shown in Figure 9, all coatings exhibited higher WCA than that of bare glass (38.3°), indicated that both PDMS and SA-reflux/PDMS coatings contributed to increase surface hydrophobicity. For PDMS coatings, increasing the number of coating layers gradually improved WCA from 101.3° to 108.5°, while CAH decreased significantly from 36.8° to 13.0°, due to the larger covered area. This indicated that PDMS matrix could provide hydrophobicity. For A1 coatings, the addition of only 1 wt% SA-reflux particles provided limited enhancement in surface roughness. By increasing number of coating layers, WCA of A1 coating increased from 102.4° to 112.2°, while CAH decreased from 19.1° to 14.6°. Although slightly improve compared to those of PDMS coatings, the roughness generated at this low SA-reflux content was insufficient to achieve superhydrophobic surface. On the other hand, A10 coatings showed significant improvement in wettability. The addition of 10 wt% SA-reflux particles developed well-defined hierarchical micro/nanostructures. By increasing number of coating layers, WCA of A10 coatings increased from 120.2° to 150.0°, while CAH decreased drastically from 27.7° to 6.2°. The A10-4 coating achieved superhydrophobic property, attributed to the synergistic effects of low surface energy imparted by stearate group on SA-modified Al_2O_3 particles and densely packed roughness that favors a Cassie–Baxter wetting state [12,39]. The multilayer coatings trapped a greater number of air pockets beneath water droplets, reducing the solid-liquid contact area and enhancing water repellency. These results indicated that achieving superhydrophobic surface required both sufficient surface roughness and low surface energy. Although long-term environmental stability was not investigated and is acknowledged as a limitation of this study, the WCA of all coating samples remained nearly unchanged throughout the experimental period under ambient condition. A symtematic investigation of environmental stability will be carried out in future work.

Self-cleaning behavior was evaluated by depositing sand particles onto the coating surface and introducing water droplets onto a tilted substrate as shown in Figure 10(a–d) [25,26]. For bare glass, PDMS-4 coating, and A1-4 coating, water droplets tended to remain pinned to surface and were difficult to roll downward, multiple droplets were required to initiate droplet motion. In case of bare glass and A1-4, the rolling droplets were unable to remove the sand particles from the

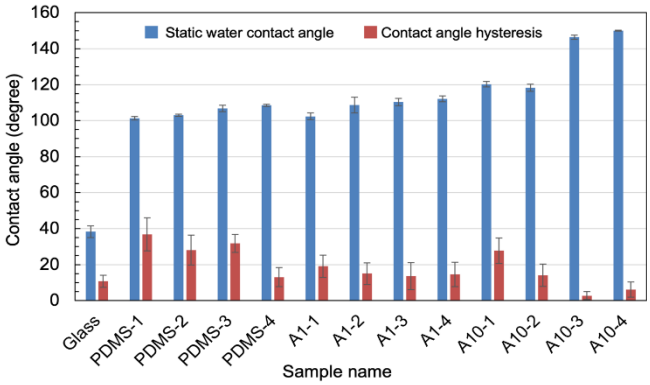

Figure 9. Static water contact angle (blue) and contact angle hysteresis (red) of the coatings.

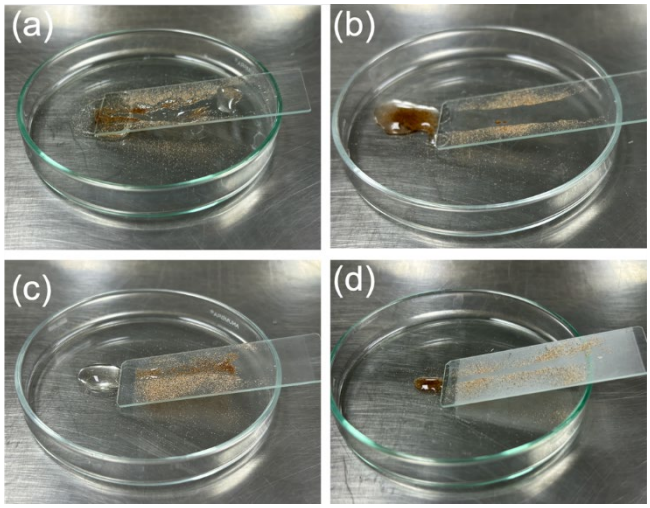

Figure 10. Self-cleaning properties after contaminated by sand particles: (a) bare glass, (b) PDMS-4, (c) A1-4, and (d) A10-4.

surface. Although droplets on PDMS-4 coating could roll downward and partially remove the sand particles along their path, noticeable droplet adhesion was still observed. These behaviors indicated relatively high droplet adhesion and insufficient surface roughness to maintain a non-wetting state. In contrast, A10-4 coating enabled a droplet to roll freely across the surface, effectively collecting and removing sand particle along its path. This behavior reflected low surface adhesion and excellent self-cleaning performance, which is characteristic of a Cassie–Baxter wetting state [12]. The superior self-cleaning performance of A10-4 coating arises from the synergistic combination of low surface energy imparted by SA-modified Al_2O_3 and the well-developed hierarchical micro/nanostructures, which trap air pockets beneath the droplet and significantly reduce solid-liquid contact.

4. Conclusions

Al_2O_3 nanoparticles were successfully modified with stearic acid. The increase of the modification temperature significantly enhanced the amount of the chemically bonded stearate on the Al_2O_3 surface. The refluxing technique yielded a higher degree of SA modification, which is approximately twice that of the soaking technique. The SA-modified Al_2O_3 was subsequently incorporated into a PDMS matrix and spray coated into glass slides. Coating containing sufficient amount of SA-modified Al_2O_3 particles developed a hierarchical micro/nano-structure in combination with the low surface energy of stearic acid, enabling superhydrophobic performance with a WCA of 150° and a CAH of 6.2°. Although increasing the coating thickness improved the wettability, it also reduced optical transmittance due to enhanced light scattering. Thus, an optimal balance transparency and super hydrophobicity is required. The resulting coating demonstrated excellent self-cleaning capability, effectively removing dust via rolling water droplets, highlighting its potential for practical applications where both water repellency and surface cleanliness are desired.

Acknowledgments

This research has received funding support from the NSRF via the Program Management Unit for Human Resources & Institutional Development, Research and Innovation [grant number B49G680122]

References

[1] X. Zhang, F. Shi, J. Niu, Y. Jiang, and Z. Wang, "Superhydrophobic surfaces: From structural control to functional application," *Journal of Materials Chemistry,* vol. 18, no. 6, pp. 621–633, 2008.

[2] W. Chen, Y. A. Fadeev, C. M. Hsieh, D. Oner, J. Youngblood, and J. T. McCarthy, "Ultrahydrophobic and ultralyophobic surfaces: Some comments and examples," *Langmuir,* vol. 15, pp. 3395–3399, 1999.

[3] Y.-Y. Quan, and L.-Z. Zhang, "Experimental investigation of the anti-dust effect of transparent hydrophobic coatings applied for solar cell covering glass," *Solar Energy Materials and Solar Cells,* vol. 160, pp. 382–389, 2017.

[4] X. Wu, and Z. Chen, "A mechanically robust transparent coating for anti-icing and self-cleaning applications," *Journal of Materials Chemistry A,* vol. 6, no. 33, pp. 16043–16052, 2018.

[5] S. Narakaew, S. Au-pree, W. Baison, S. Thungprasert, I. Wattalo, P. Jaipor, T. Promanan, S. Sukdee, P. Santakij, C. Chanogkun, K. Ruttananteeranwichien, A. Chaisena, P. Apichai, and P. Napakaew, "The finished polyester fabric with hot NH_4OH pretreatment and mixed ZnO-$Zn(OH)_2$ nanoparticles for hydrophobic property," *Journal of Metals, Materials and Minerals,* vol. 32, pp. 109–117, 2022.

[6] H. H. I. Eltigani, and Y. Boonyongmaneerat, "Progress of water desalination applications based on wettability and surface characteristics of graphene and graphene oxide: A review," *Journal of Metals, Materials and Minerals,* vol. 32, pp. 15–26, 2022.

[7] S. S. Latthe, R. S. Sutar, V. S. Kodag, A. K. Bhosale, A. M. Kumar, K. K, Sadasivuni, R. Xing, and S. Liu, "Self – cleaning superhydrophobic coatings: Potential industrial applications," *Progress in Organic Coatings,* vol. 128, pp. 52–58, 2019.

[8] P. Wang, M. Chen, H. Han, X. Fan, Q. Liu, and J. Wang, "Transparent and abrasion-resistant superhydrophobic coating with robust self-cleaning function in either air or oil," *Journal of Materials Chemistry A,* vol. 4, no. 20, pp. 7869–7874, 2016.

[9] A. Matin, U. Baig, S. Akhtar, N. Merah, M. A. Gondal, A. H. Bake, and A. Ibrahim, "UV-resistant and transparent hydrophobic surfaces with different wetting states by a facile dip-coating method," *Progress in Organic Coatings,* vol. 136, p. 105192, 2019.

[10] A. Nakajima, K. Hashimoto, and T. Watanabe, "Recent studies on super-hydrophobic films," *Monatshefte fur Chemie,* vol. 132, pp. 31–41, 2001.

[11] R. N. Wenzel, "Resistance of solid surfaces to wetting by water," *Industrial and engineering chemistry,* vol. 28, pp. 988–994, 1936.

[12] A. B. D. Cassie, and S. Baxter, "Wettability of porous surfaces," *Transactions of the Faraday society,* vol. 40, pp. 546–551, 1944.

[13] P. N. Manoudis, and I. Karapanagiotis, "Modification of the wettability of polymer surfaces using nanoparticles," *Progress in Organic Coatings,* vol. 77, no. 2, pp. 331–338, 2014.

[14] D. Ebert, and B. Bhushan, "Transparent, superhydrophobic, and wear-resistant coatings on glass and polymer substrates using SiO_2, ZnO, and ITO nanoparticles," *Langmuir,* vol. 28, no. 31, pp. 11391–11399, 2012.

[15] L. Xu, R. G. Karunakaran, J. Guo, and S. Yang, "Transparent, superhydrophobic surfaces from one-step spin coating of hydrophobic nanoparticles," *ACS Applied Materials & Interfaces,* vol. 4, no. 2, pp. 1118–1125, 2012.

[16] X. Sun, J. Xie, J. Zhang, M. Sang, Y. Li, P. Lyu, D. Chen, and H. Zhou, "Hydrophobic Al_2O_3/SiO_2/PDMS composite coatings for anti-corrosion application of 304 stainless-steel," *Journal of Inorganic and Organometallic Polymers and Materials,* vol. 32, no. 11, pp. 4237–4249, 2022.

[17] R. Fateh, R. Dillert, and D. Bahnemann, "Preparation and characterization of transparent hydrophilic photocatalytic TiO_2/SiO_2 thin films on polycarbonate," *Langmuir,* vol. 29, no. 11, pp. 3730–3739, 2013.

[18] Y. Shen, K. Li, H. Chen, Z. Wu, and Z. Wang, "Superhydrophobic F-SiO_2@PDMS composite coatings prepared by a two-step spraying method for the interface erosion mechanism and anti-corrosive applications," *Chemical Engineering Journal,* vol. 413, p. 127455, 2021.

[19] F. Su, and K. Yao, "Facile fabrication of superhydrophobic surface with excellent mechanical abrasion and corrosion resistance on copper substrate by a novel method," *ACS Applied Materials & Interfaces,* vol. 6, no. 11, pp. 8762–8770, 2014.

[20] M. Uhl, G. Schoeters, E. Govarts, W. Bil, T. Fletcher, L. S. Haug, R. Hoogenboom, C. Gundacker, X. Trier, M. F. Fernandez, A. C. Calvo, M. E. López, D. Coertjens, T. Santonen, L. P. Murínová, D. Richterová, K. De Brouwere, I. Hauzenberger, M. Kolossa-Gehring, and Þ. I. Halldórsson "PFASs: What can we learn from the european human biomonitoring initiative HBM4EU," *International Journal of Hygiene and Environmental Health,* vol. 250, p. 114168, 2023.

[21] B. Zhang, W. Xu, Q. Zhu, and B. Hou, "Scalable, fluorine free and hot water repelling superhydrophobic and superoleophobic coating based on functionalized Al_2O_3 nanoparticles," *Journal of Materials Science & Technology,* vol. 66, pp. 74–81, 2021.

[22] L. Zhang, C.-H. Xue, M. Cao, M.-M. Zhang, M. Li, and J.-Z. Ma, "Highly transparent fluorine-free superhydrophobic silica nanotube coatings," *Chemical Engineering Journal,* vol. 320, pp. 244–252, 2017.

[23] A. P. Desbois, and V. J. Smith, "Antibacterial free fatty acids: activities, mechanisms of action and biotechnological potential," *Applied Microbiology and Biotechnology,* vol. 85, no. 6, pp. 1629–1642, 2010.

[24] A. Jiménez, M. J. Fabra, P. Talens, and A. Chiralt, "Effect of lipid self-association on the microstructure and physical properties of hydroxypropyl-methylcellulose edible films containing fatty acids," *Carbohydrate Polymers,* vol. 82, pp. 585–593, 2010.

[25] H. Li, L. Xin, K. Zhang, X. Yin, and S. Yu, "Fluorine-free fabrication of robust self-cleaning and anti-corrosion superhydrophobic coating with photocatalytic function for enhanced anti-biofouling property," *Surface and Coatings Technology,* vol. 438, p. 128406, 2022.

[26] Y. Feng, S. Chen, and Y. Frank Cheng, "Stearic acid modified zinc nano-coatings with superhydrophobicity and enhanced antifouling performance," *Surface and Coatings Technology,* vol. 340, pp. 55–65, 2018.

[27] Y. Li, and W. Weng, "Surface modification of hydroxyapatite by stearic acid: Characterization and in vitro behaviors," *Journal of Materials Science: Materials in Medicine,* vol. 19, no. 1, pp. 19–25, 2008.

[28] H. Teisala, P. Baumli, S. A. L. Weber, D. Vollmer, and H. J. Butt, "Grafting silicone at room temperature-a transparent, scratch-resistant nonstick molecular coating," *Langmuir,* vol. 36, no. 16, pp. 4416–4431, 2020.

[29] S. Martin, and B. Bhushan, "Transparent, wear-resistant, superhydrophobic and superoleophobic poly(dimethylsiloxane) (PDMS) surfaces," *Journal of Colloid and Interface Science,* vol. 488, pp. 118–126, 2017.

[30] E. J. Park, Y. K. Cho, D. H. Kim, M. G. Jeong, Y. H. Kim, and Y. D. Kim, "Hydrophobic polydimethylsiloxane (PDMS) coating of mesoporous silica and its use as a preconcentrating agent of gas analytes," *Langmuir,* vol. 30, no. 34, pp. 10256–10262, 2014.

[31] L. Hu, Z. Pu, Y. Tian, X. Zheng, J. Cheng, and J. Zhong, "Preparation and properties of fluorinated silicon two-component polyurethane hydrophobic coatings," *Polymer International,* vol. 69, no. 5, pp. 448–456, 2020.

[32] S. Zheng, D. A. Bellido-Aguilar, Y. Huang, X. Zeng, Q. Zhang, and Z. Chen, "Mechanically robust hydrophobic bio-based epoxy coatings for anti-corrosion application," *Surface and Coatings Technology,* vol. 363, pp. 43–50, 2019.

[33] S. Sutha, S. Suresh, B. Raj, and K. R. Ravi, "Transparent alumina based superhydrophobic self–cleaning coatings for solar cell cover glass applications," *Solar Energy Materials and Solar Cells,* vol. 165, pp. 128–137, 2017.

[34] S. Mishra, N. G. Shimpi, and A. D. Mali, "Influence of stearic acid treated nano-$CaCO_3$ on the properties of silicone nano-composites," *Journal of Polymer Research,* vol. 18, no. 6, pp. 1715–1724, 2011.

[35] Z. Liu, L. Yao, X. Pan, Q. Liu, and H. Huang, "A green and facile approach to the efficient surface modification of alumina nanoparticles with fatty acids," *Applied Surface Science,* vol. 447, pp. 664–672, 2018.

[36] M. E. Karaman, D. A. Antelmi, and R. M. Pashley, "The production of stable hydrophobic surfaces by the adsorption of hydrocarbon and fluorocarbon carboxylic acids onto alumina substrates," *Colloids and Surfaces A: Physicochemical and Engineering Aspects,* vol. 182, pp. 285–298, 2001.

[37] J. Chandradass, and M. Balasubramanian, "Sol–gel processing of alumina fibres," *Journal of Materials Processing Technology,* vol. 173, no. 3, pp. 275–280, 2006.

[38] L. Zhang, L. Chen, H. Wan, J. Chen, and H. Zhou, "Synthesis and tribological properties of stearic acid-modified anatase (TiO_2) nanoparticles," *Tribology Letters,* vol. 41, no. 2, pp. 409–416, 2010.

[39] L. Feng, H. Zhang, P. Mao, Y. Wang, and Y. Ge, "Superhydrophobic alumina surface based on stearic acid modification," *Applied Surface Science,* vol. 257, pp. 3959–3963, 2011.

[40] M. Zhang, M. Zhao, R. Chen, J. Liu, Q. Liu, J. Yu, R. Li, P. Liu, and J. Wang, "Fabrication of the pod-like KCC-1/TiO_2 superhydrophobic surface on AZ31 Mg alloy with stability and photocatalytic property," *Applied Surface Science,* vol. 499, p. 143933, 2020.

[41] F. Kimura, J. Umemura, and T. Takenaka, "FTIR-ATR studies on Langmuir-Blodgett films of stearic acid with 1-9 monolayers," *Langmuir,* vol. 2, pp. 96–101, 1986.

[42] Y. Gan, M. Zhao, S. Zhao, Z. Su, J. Xie, L. Yang, and T.-J. Wang, "Increased stearic acid grafting density on silica nanoparticles via alumina-activation," *Applied Surface Science,* vol. 678, p. 161077, 2024.

[43] X.-X. Zhang, B.-B. Xia, H.-P. Ye, Y.-L. Zhang, B. Xiao, L.-H. Yan, H.-B. Lv, and B. Jiang, "One-step sol–gel preparation of PDMS–silica ORMOSILs as environment-resistant and crack-free thick antireflective coatings," *Journal of Materials Chemistry,* vol. 22, no. 26, pp. 13132–13140, 2012.

[44] G. Mie, "Beiträge zur optik trüber medien, speziell kolloidaler metallösungen," *Annalen der Physik,* vol. 330, no. 3, pp. 377-445, 1908.

[45] P. Spinelli, M. A. Verschuuren, and A. Polman, "Broadband omnidirectional antireflection coating based on subwavelength surface Mie resonators," *Nature Communications,* vol. 3, p. 692, 2012.